

# Enhancing Tumor Microstructural Quantification With Machine Learning and Diffusion-Relaxation MRI

Carlos Macarro, MSc,<sup>1</sup> Kinga Bernatowicz, PhD,<sup>1</sup>
Alonso Garcia-Ruiz, MSc,<sup>1</sup> Garazi Serna, PhD,<sup>1</sup>
Camilo Monreal-Agüero, MSc,<sup>1</sup> Sara Simonetti, MD, PhD,<sup>1</sup>
Matteo Figini, PhD,<sup>2</sup> Juan Francisco Corral, MSc,<sup>3,4</sup>
Valezka Garay, MSc,<sup>5</sup> Marta Vidorreta, PhD,<sup>6</sup>
Pablo García-Polo García, PhD,<sup>7</sup> Xavier Merino, MD,<sup>3,4</sup>
Richard Mast, MD,<sup>3,4</sup> Núria Roson, MD, PhD,<sup>3,4</sup>
Maria Vieito, MD,<sup>1,8</sup> Manuel Escobar, MD,<sup>3,4</sup>
Daniel C. Alexander, PhD,<sup>2</sup> Rodrigo Toledo, PhD,<sup>1</sup>
Paolo Nuciforo, MD, PhD,<sup>1</sup> Elena Garralda, MD,<sup>1,8</sup>
Raquel Perez-Lopez, MD, PhD,<sup>1\*</sup> and Francesco Grussu, PhD<sup>1\*</sup>

#### To the Editor:

Diffusion MRI (dMRI) enables tumor characterization, providing metrics of cellular properties that could become powerful biomarkers. However, the number and type of properties that can be resolved depends on the number of images encompassing the dMRI protocol. Long acquisition times are often required to support accurate microstructural signal models, implying that these often remain relegated to research studies.

Here, we investigated whether machine learning (ML) can bridge the gap between routine, clinical dMRI and more advanced quantitative methods, such as joint diffusion-relaxation (DR) imaging. We studied the ML-based prediction of advanced DR parametric maps from short dMRI protocols that are feasible in the clinic, focusing on pelvic and abdominal imaging of advanced solid tumors.

#### **Concise Methods**

Complete methods in Data S1.

## Data Acquisition

Data from two scanners were analyzed (1.5T Siemens Avanto; 3T GE SIGNA Pioneer), which included anatomical T2w and DR imaging (21 contrasts: 7 *b*-values acquired at 3 TE each). To simulate a more clinical protocol, we extracted a subset of five images (the five lowest *b*-values acquired at the minimum TE, referred to as "clinical protocol"). Conversely, the full set of 21 DR measurements is referred to as "advanced protocol." DR images were denoised and corrected for Gibbs ringing and motion. Tumors >1 cm in diameter were manually segmented on the T2w scan and co-registered to DR space. Biopsies from one of the imaged tumors were also collected.

#### Signal Models

**CLINICAL METRICS.** From the clinical protocol, we fitted a mono-exponential signal decay  $S = S_0 e^{-bADC}$  on three scenarios: 1)

the whole dMRI clinical set of images, obtaining the Apparent Diffusion Coefficient (ADC) and the proton density  $S_0$ ; 2) the lowest b-values (0, 50,  $100 \, \text{s/mm}^2$ ), obtaining a vascular-driven pseudo-ADC (ADC<sub>fast</sub>); 3) the highest b-values (100, 400, 900  $\text{s/mm}^2$ ), obtaining an average, tissue ADC (ADC<sub>slow</sub>). Moreover, a proxy for the vascular, pseudo-diffusion signal fraction was obtained by combining the  $S_0$  estimates from the first and last fits as  $F \approx 1 - \frac{S_{0,\text{slow}}}{S_0}$ .

**ADVANCED METRICS.** The advanced protocol was taken as reference. It enables fitting a complex signal model, jointly capturing T2 relaxation, intravoxel incoherent motion (IVIM) and tissue diffusion, distinguishing between Gaussian/non-Gaussian diffusion. The used DR signal representation will be referred as T2-IVIM-Kurtosis and is:  $S = S_0 \left( f e^{-bD_v - \frac{TE}{12s}} + (1-f) e^{-bD_t + \frac{1}{6}K(bD_t)^2 - \frac{TE}{72s}} \right) \ (v/t \ \text{indicate})$  vascular/tissue properties).

## **Prediction Strategies**

We studied two predictions strategies (Fig. 1a): 1) signal-to-signal predicts the DR signals of the advanced protocol given the clinical protocol, so that T2-IVIM-Kurtosis can be fitted on such predicted signals; 2) maps-to-maps predicts directly T2-IVIM-Kurtosis metrics from ADC<sub>fast</sub>, ADC<sub>slow</sub>, F. Both approaches were implemented using seven algorithms and deployed on a leave-one-out fashion. 6/7 algorithms worked voxel-wise, while one patch-wise. All implementations are freely available online (https://github.com/carlosmacarro/clinical2advanced).

#### **Prediction Evaluation**

We assessed the quality of the predicted T2-IVIM-Kurtosis metrics through per-patient bias and dispersion indices (BI, DI), with  $BI = P_{50}(E)$  and  $DI = (P_{75}(E) - P_{25}(E))$ , where  $P_X$  is the Xth percentile and  $E = \frac{\text{prediction-ground truth}}{\text{ground truth}}$  the relative error. Pixel-level correlations between reference/estimated parameters were also computed.

#### Training Set Size

We assessed the impact of the training set size on the prediction by systematically reducing the number of patients included in the training set.

### Results

Thirty-two patients with advanced solid tumors (Fig. S1 in the Supplemental Material) were included (15 males,  $64.31 \pm 10.73$  years), 16/32 scanned with the Siemens system (cohort 1) and 16/32 with the GE system (cohort 2). In *signal-to-signal*, all algorithms capture salient characteristics of the diffusion-T2 decay (Fig. S2 in the Supplemental Material) and of anatomical features (mean relative errors below 12%; Fig. 1b; Table S1 and Figs. S3 and S4 in the Supplemental Material). T2-IVIM-Kurtosis maps fitted to the *signal-to-*

This is an open access article under the terms of the Creative Commons Attribution-NonCommercial-NoDerivs License, which permits use and distribution in any medium, provided the original work is properly cited, the use is non-commercial and no modifications or adaptations are made.

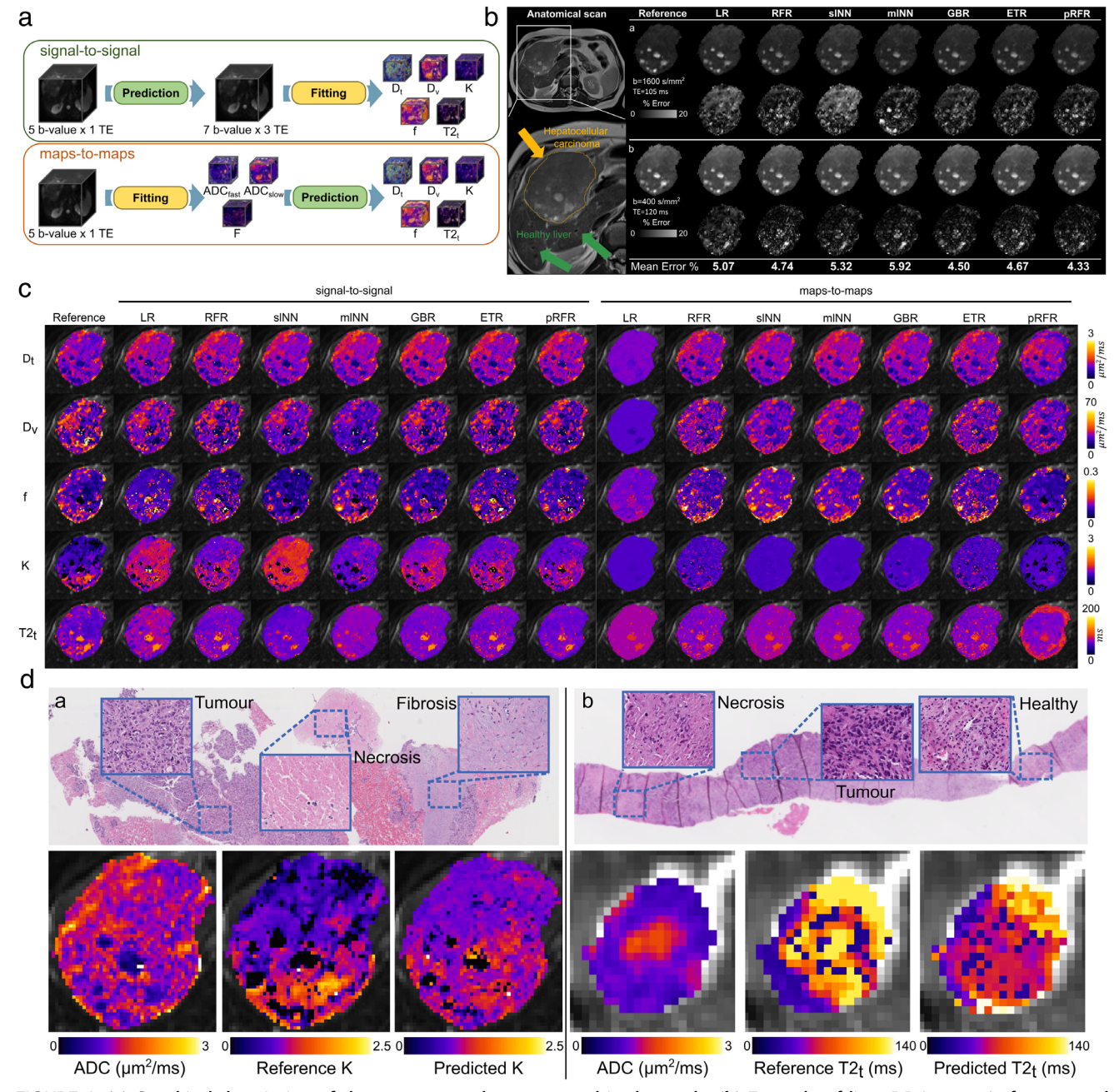


FIGURE 1: (a) Graphical description of the two approaches compared in the study. (b) Example of liver DR images (reference and predicted) form a 65-year-old female patient (cohort 1) who suffered from a primary hepatocellular carcinoma, alongside percentage relative error maps and mean percentage relative error of the entire hepatocellular carcinoma. An orange arrow indicates the hepatocellular carcinoma and green arrows point toward the healthy liver. (b.a) Images acquired at  $b = 1600 \text{ s/mm}^2$  and TE = 105 msec with unseen predictions and error maps; (b.b) images acquired at  $b = 400 \text{ s/mm}^2$  and TE = 120 msec with unseen predictions and error maps. (c) Example of reference and predicted T2-IVIM-Kurtosis maps obtained from both signal-to-signal and maps-to-maps strategies (images from the same hepatocellular carcinoma seen in b). (d.a) H&E from a biopsy of the hepatocellular carcinoma seen in b and c, alongside ADC map and reference and predicted kurtosis (K) maps. (d.b) Biopsy of liver metastasis of a 47-year-old female melanoma patient (cohort 2) alongside the ADC map and reference and predicted T2t maps of the entire lesion. In both cases, the H&E shows the existence of different microstructural environments within the tumor, a finding that is line with the heterogeneity also seen on maps such as ADC, K or T2t. LR = linear regression; RFR = random forest regressor; ETR = extra trees regressor; GBR = gradient boosting regressor; slNN = single-layer neural network; mlNN = multi-layer neural network.

signal output show less variability between algorithms than those predicted from maps-to-maps. K and T2t are qualitatively worse in maps-to-maps (Fig. 1c). Biopsies reveals the existence of a variety of intra-tumor cellular characteristics (eg, active cancer and necrosis). All MRI metrics (both clinical and advanced) reveal intra-tumoral

heterogeneity, mirroring the histological ground truth. However, advanced metrics such as K and T2t enable the quantification of non-Gaussian diffusion and T2 relaxation, potentially giving extra information than protocols not including high b and multiple TE (Fig. 1d; Fig. S5 in the Supplemental Material).

February 2025 1019

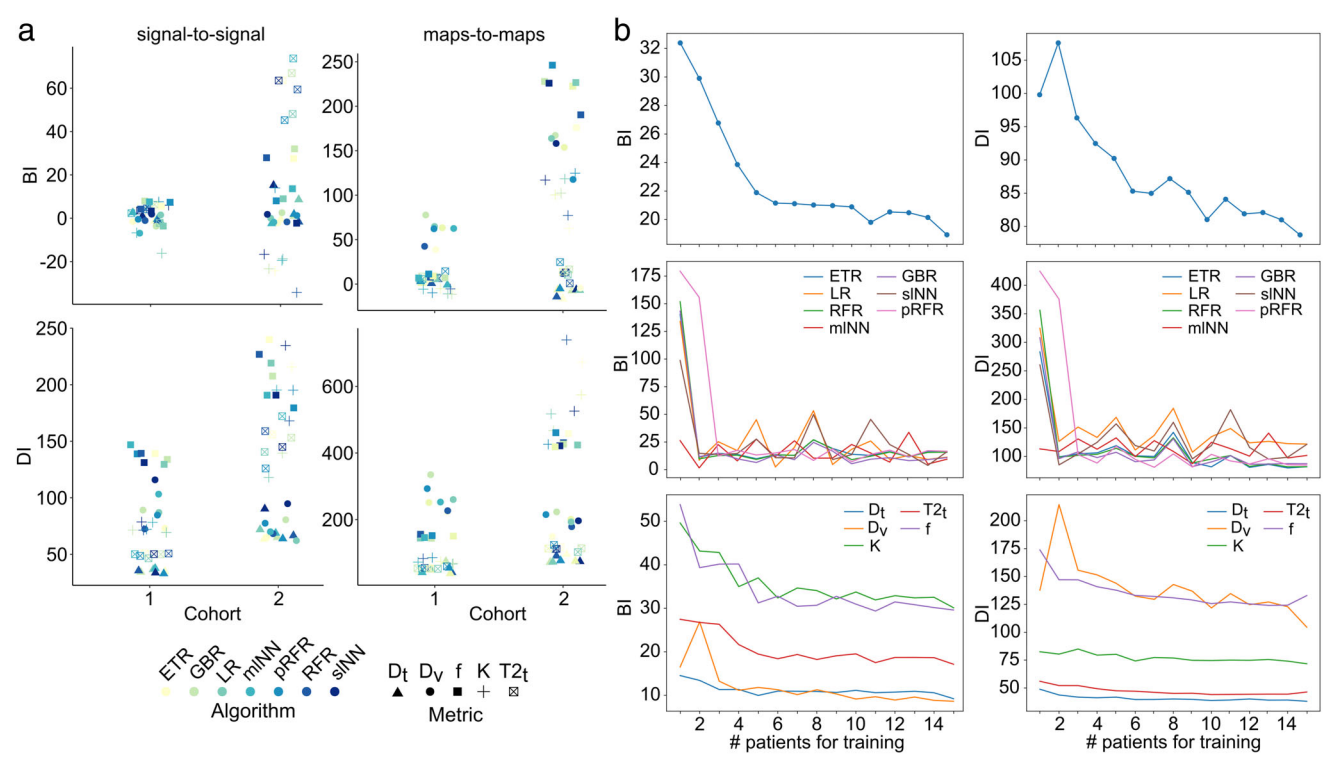


FIGURE 2: (a) Distribution of mean BI and DI of each predicted T2-IVIM-Kurtosis metric/algorithm combination, for both signal-to-signal and maps-to-maps prediction strategies. Metrics are differentiated by shape and algorithms by color. Points show a trend to cluster by metric rather than algorithm. Both BI and DI are lower (better) for the signal-to-signal approach (note the different y-axis range for signal-to-signal vs. maps-to-maps). Cohort 2 presents worse BI and DI for both strategies. (b) Impact of the training set size on signal-to-signal predictions. On top: overall mean BI and DI as a function of the training size. In the middle: BI and DI for every algorithm as a function of the training set size. On the bottom: BI and DI of every DR metric as a function of the training set size. LR = linear regression; RFR = random forest regressor; ETR = extra trees regressor; GBR = gradient boosting regressor; sINN = single-layer neural network; mINN = multi-layer neural network.

Mean BI and DI are lower for signal-to-signal than maps-to-maps. A greater variation is seen between metrics than between algorithms, and such variation is pronounced in maps-to-maps. In general, ML algorithms achieve better performances in cohort 1 than 2 (lower BI and DI; Fig. 2a; Figs. S6 and S7 in the Supplemental Material). No statistical differences between algorithms are seen, for a fixed prediction strategy (Fig. S8 in the Supplemental Material). Pixel-level correlations between reference and predicted DR signals are above 0.8 for both cohorts but lower correlations are seen between reference and predicted metrics (Fig. S9 in the Supplemental Material).

BI and DI decrease as the training size increases. It stabilizes around N=5 patients. mlNN exhibits low BI and DI even with only N=2 training cases. DI's fluctuations in the range 5–15 patients are mainly caused by  $D_{\nu}$  (Fig. 2b; Fig. S11 in the Supplemental Material).

# Discussion

We investigated whether ML can enhance the amount of information on tissue microstructure that can be extracted from clinically viable dMRI scans. It appears feasible to gain insight on DR properties from shorter dMRI protocols at fixed TE in advanced solid tumors, using small training cohorts. To achieve this, predicting rich DR protocols and then fitting advanced signal models on the predicted signals provides substantially better performances than

predicting DR maps directly. In practice, training cohorts as small as N=5 scans may suffice for this purpose, and independently of the specific algorithm used for prediction. Therefore, we recommend that efforts of the community should focus on the signal prediction, rather than on the unseen parametric maps.

We acknowledge some limitations of our approach. First, we did not consider advanced deep learning algorithms, for example, vision transformers, which we will study in future work. Second, here we only provide a first pilot demonstration, which we aim to confirm in larger cohorts, and in data from more MRI scanners and acquisition protocols, beyond DR imaging.

# Conclusions

For DR quantification in abdominal and pelvic solid tumors, using ML to enhance the information that can be extracted from clinical dMRI protocols appears feasible, with practical training sets of as few as five scans.

# **Acknowledgments**

We thank the whole medical oncology, radiology, pathology, molecular biology, clinical trial, and IT teams at the Vall d'Hebron Campus. We would also like to express our sincere gratitude to all patients and their families for dedicating their time to research. VHIO acknowledges the State Agency for Research (Agencia Estatal

1020 Volume 61, No. 2

de Investigación) for the financial support as a Center of Excellence Severo Ochoa (CEX2020-001024-S/AEI/10.13039/501100011 033), the Cellex Foundation for providing research facilities and equipment and the CERCA Programme from the Generalitat de Catalunya for their support. This research has been supported by PREdICT, sponsored by AstraZeneca. This study has been cofunded by the European Regional Development Fund/European Social Fund "A way to make Europe" (to R.P.L.). RPL is supported by "la Caixa" Foundation, the Prostate Cancer Foundation (18YOUN19), a CRIS Foundation Talent Award (TALENT19-05), the FERO Foundation through the XVIII Fero Fellowship for Oncological Research, the Instituto de Salud Carlos III-Investigación en Salud (PI18/01395 and PI21/01019), the Asociación Española Contra el Cancer (AECC) (PRYCO211023SERR) and the Agency for Management of University and Research Grants of Catalonia (AGAUR) (2023PROD00178). This research has been funded by the CaixaResearch Advanced Oncology Research Program supported by "La Caixa" Foundation (to R.P.L.). The project that gave rise to these results received the support of a fellowship from "la Caixa" Foundation (ID 100010434). The fellowship code is "LCF/BQ/ PR22/11920010", funding F.G. This research has received support from the Beatriu de Pinós Postdoctoral Program from the Secretariat of Universities and Research of the Department of Business and Knowledge of the Government of Catalonia, and the support from the Marie Sklodowska-Curie COFUND program (BP3, contract number 801370; reference 2019 BP 00182) of the H2020 program (to K.B.). C.M. is supported by the Asociación Española Contra el Cancer (PRYCO211023SERR). VHIO is also grateful to the Generalitat de Catalunya, Comissió Interdepartamental de Recerca i Innovació Tecnològica.

## **Conflict of Interest**

Data acquisition was sponsored by AstraZeneca (AZ). MVid works for Siemens. PGPG works for GE. KB worked as a researcher at VHIO, and is now an employee of AZ. AZ, Siemens and GE did not influence the design of the study; the experiments and analysis; the interpretation of data and results; manuscript writing; the

Macarro et al.: Diffusion-relaxation MRI enhancement in cancer

decision to submit the manuscript in its present form for publication; or any other aspect concerning this article.

<sup>1</sup>Vall d'Hebron Institute of Oncology (VHIO), Vall d'Hebron Barcelona Hospital Campus, Barcelona, Spain

<sup>2</sup>Centre for Medical Image Computing, Department of Computer Science, University College London, London, UK

<sup>3</sup>Department of Radiology, Hospital Universitari Vall d'Hebron, Barcelona, Spain

<sup>4</sup>Institut de Diagnòstic per la Imatge (IDI), Barcelona, Spain <sup>5</sup>PET/MR Unit, CETIR-Ascires, Barcelona, Spain

<sup>6</sup>Siemens Healthineers, Madrid, Spain

<sup>7</sup>GE HealthCare, Madrid, Spain

<sup>8</sup>Medical Oncology Service, Vall d'Hebron Barcelona Hospital Campus, Vall d'Hebron Institute of Oncology (VHIO), Barcelona, Spain

Raquel Perez-Lopez and Francesco Grussu are senior and corresponding authors.

## References

- Grussu F, Bernatowicz K, Casanova-Salas I, et al. Diffusion MRI signal cumulants and hepatocyte microstructure at fixed diffusion time: Insights from simulations, 9.4T imaging, and histology. Magn Reson Med 2022; 88:365-379.
- Panagiotaki E, Chan RW, Dikaios N, et al. Microstructural characterization of normal and malignant human prostate tissue with vascular, extracellular, and restricted diffusion for cytometry in tumours magnetic resonance imaging. Invest Radiol 2015;50(4):218-227.
- Jiang X, Xu J, Gore JC. Mapping hepatocyte size in vivo using temporal diffusion spectroscopy MRI. Magn Reson Med 2020;84(5):2671-2683.
- Alexander DC, Zikic D, Ghosh A, et al. Image quality transfer and applications in diffusion MRI. Neuroimage 2017;152:283-298.

DOI: 10.1002/jmri.29484

Evidence Level: 3

Technical Efficacy: Stage 1

February 2025 1021